Evidence of a small exciton in the $Ba_{1-x}K_xBiO_3$ superconductor and its relationship with superconductivity

Y. Y. Wang*
Department of Materials Science and Engineering, Northwestern University, Evanston, Illinois 60208 and IBM, Zip 40E, 2070 Route 52, Hopewell Junction, New York 12533-6531

P. D. Han
Department of Materials Science and Engineering, University of Illinois, Urbana, Illinois 61801
(Received 3 October 2001; revised manuscript received 26 August 2002; published 16 January 2003)

The effective mass of a free-carrier plasmon is measured by momentum-resolved electron-energy-loss spectroscopy. The effective mass of the plasmon is heavy along the [100] direction and light along the [110] direction in the optimal doped regime, where T_c is highest. The anisotropy of the effective mass between [100] and [110] decreases with increasing doping and decreasing of T_c. In the overdoped regime with T_c almost zero (normal metal state), the effective mass of the free-carrier plasmon becomes isotropic. A linear correlation between T_c and the effective mass difference along the two orientations is extracted from the experimental data. The dispersion of the plasmon for the optimal doped material cannot be explained by the band structure alone, but that for the overdoped material is consistent with the band-structure calculation. This indicates that the effective mass is strongly renormalized along [100] by an additional interaction in the optimally doped material of the highest T_c. Of related interest is a group of small excitons in the parent compound of $Ba_{1-x}K_xBiO_3$ (BKBO), $BaBiO_3$, with assigned symmetries that are *s* wave (optically forbidden) at 4.2 eV, *p* wave at 2.1 eV (optically allowed), and *d* wave at 0.5 eV (optically forbidden). We propose a mixing state of free carriers and small excitons to explain the anisotropic dispersion for the optimally doped regime and a free-carrier state free of small excitons for the overdoped material (normal metal state). The linear correlation between T_c and mass renormalization provides insight that the superconductivity of BKBO may be related to electronic structure, possibly to the small exciton or WZK (Wang-Zhang-Klein) exciton.

DOI: 10.1103/PhysRevB.67.024505 PACS number(s): 74.70.−b, 71.18.+y, 78.20.−e

I. INTRODUCTION

After more than 10 years of research, the mechanism of high-temperature superconductivity in oxide materials still remains elusive. The electronic structure of oxide superconductors has been under intense investigation in search for an alternative mediating boson for the formation of Cooper pairs in this kind of superconductivity. In the general class of oxide superconductors, the $Ba_{1-x}K_xBiO_3$ (BKBO) superconductor is of strategic importance for understanding the mechanism of high-T_c superconductivity, because it does not contain CuO_2 planes.[1–3]

One of the important parameters of the electronic structure is the effective mass of its ''free-carrier'' plasmon or exciton, which can be measured by angle-resolved electron-energy-loss spectroscopy, and is given by the two lowest-order terms in the expansion,

$$E(q)=E_0+\frac{\hbar^2}{2m^*}q^2, \tag{1}$$

where E_0 is the excitation energy at $q\rightarrow 0$, q is the momentum transfer, and m^* is the effective mass of the excitation (free-carrier plasmon or exciton).

Recently, small excitons were discovered in the parent compound of BKBO, $BaBiO_3$, as well as in a cuprate parent compound, $Sr_2CuO_2Cl_2$. It is found that the effective mass of the small exciton in $BaBiO_3$ is highly anisotropic, with higher dispersion along the [110] direction, and almost zero dispersion along the [100] direction.[4,5] The question is whether a small exciton coexists with the free carrier in the superconducting state of BKBO.

In order to understand how the electronic structure is related to superconductivity, we investigated the electronic structure over a wide range of doping material, from optimum doping to overdoping. The highest dopant of K in BKBO was achieved to 0.73 with T_c as low as 2 K. By angle-resolved electron-energy-loss spectroscopy (EELS), we report a clear difference in the electronic structure of BKBO in terms of dispersion of the free-carrier plasmon between the optimally doped material, where T_c is the highest, and the overdoped material, where T_c is almost zero.

The anisotropic dispersion was compared with a band structure calculation. It was found that at optimal doping, where T_c is the highest, the dispersion of the plasmon cannot be explained by a conventional band structure calculation but can be explained by a mixing of the plasmon with small excitons of similar symmetry. In the overdoped regime, where T_c is almost zero, the dispersion of the plasmon is more isotropic and is consistent with band structure theory without additional modifications. Combining these results with the results on the small exciton in $BaBiO_3$ and $Sr_2CuO_2Cl_2$, we propose a model of mixing the small exciton and free carrier in the optimal doped case. Based on that picture and the linear correlation between T_c and the

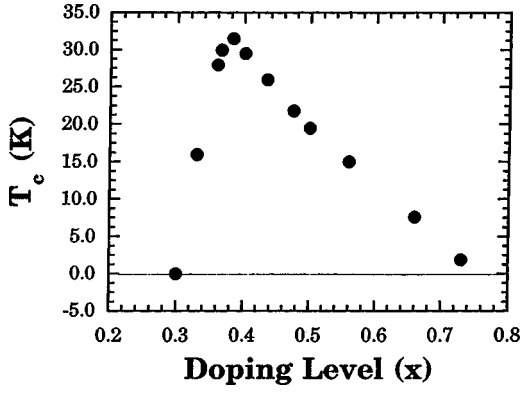

FIG. 1. T_c vs x, the doping level for $Ba_{1-x}K_xBiO_3$. T_c drops with increasing K concentration. At $x=0.73$, it is below 4 K, which makes the material more or less like a normal metal.

effective-mass renormalization, we conclude that the superconductivity in BKBO may be related to the small exciton, which is referred as a WZK exciton, initially investigated by Wang, Zhang, and Klein.[4,5]

II. EXPERIMENT

In a previous report of BKBO material synthesis using conventional methods the highest doping achieved was to $x=0.50$, with a T_c of ~20 K.[6] In order to push doping even further, we employed an electrochemical growth method[7] and covered a wide doping range for BKBO single crystals, where the highest doping achieved was $x=0.73$ with a decreased T_c of less than 2 K.[8] Figure 1 shows the variation of T_c with different doping levels. The T_c of the samples with doping levels below $x=0.5$ is consistent with prior work.[6] The detailed description of the preparation method for the new material is described elsewhere.[8]

Transmission electron microscopy (TEM) specimens of single-crystalline BKBO were prepared by mechanically polishing bulk slices to about 5 μm thickness and subsequently ion-beam thinning to ~1000 Å at liquid-nitrogen temperature to reduce ion-beam damage to the sample during the milling. Energy-loss spectra were obtained using a cold-field emission gun TEM (Hitachi HF-2000) equipped with a Gatan 666 parallel detection electron-energy-loss spectrometer (PEELS). All spectra were acquired at room temperature. The peak width of the unscattered beam is ~0.4 eV. The zero-loss peak was removed by fitting it with an asymmetric Lorentzian function and multiple scattering in the energy-loss spectra was removed to the third order.[9] The peak position of free-carrier plasmon was determined by peak-fitting method, which gives more accurate results. The accuracy of the fitting method was discussed in Ref. 9.

III. RESULTS

Angle-resolved electron-energy-loss spectra for the transferred wave vector **q** along [100] and [110] were measured on three different doped samples with doping levels of $x=0.38$, 0.50, and 0.73, and with T_c values of 32, 19, and 2 K, respectively.

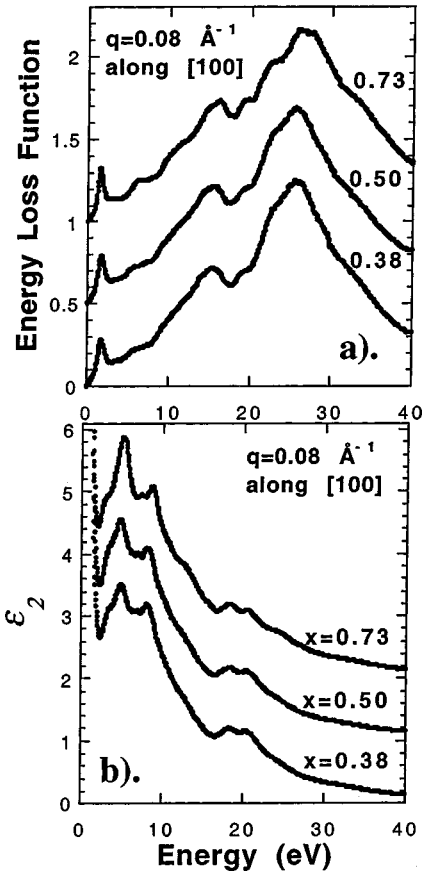

FIG. 2. (a) Energy-loss function of different $x=0.38$, 0.50, 0.73 along the [100] direction with $q=0.08$ Å^{-1}. Multiple scattering is removed from the loss spectrum and the loss function between 1 eV is fitted with a Drude model on the background of a broad excitation near that region. (b) Imaginary part of dielectric function obtained from *K-K* analysis of loss function. Increasing K concentration seems to increase the intensity of the excitation at 5 eV.

The energy-loss functions at small momentum transfer of 0.08 Å^{-1} with $x=0.38$, 0.50, and 0.73 are shown in Fig. 2(a). The multiple scattering is removed for each spectrum. The energy-loss function below 1 eV is fitted with a Drude model on a broad excitation near that region. The imaginary part of dielectric function is obtained through K-K (Kramers-Kronig) analysis by assuming ε_0 goes to infinity at zero energy. The intensity of excitation at 5 eV increases with increasing K concentration.

The width of free-carrier plasmon peak for different concentrations of K with $q=0.08$ Å^{-1} along [100] is fitted by a Drude model with a broad background excitation. It is shown in Fig. 3 as square point. The width decreases with increasing K concentration. In addition, the free-carrier plasmon intensity in the loss function for different K concentration is also plotted in Fig. 3 as circle point. The intensity increases with increasing K concentration. In a previous report[10] with EELS on polycrystalline, we did not observe a significant difference in plasmon intensity between $x=0.40$ and $x=0.50$. The difference between current data and previous data can be attributed to two reasons: (1) In the previous measurement with a polycrystalline sample, the orientation is

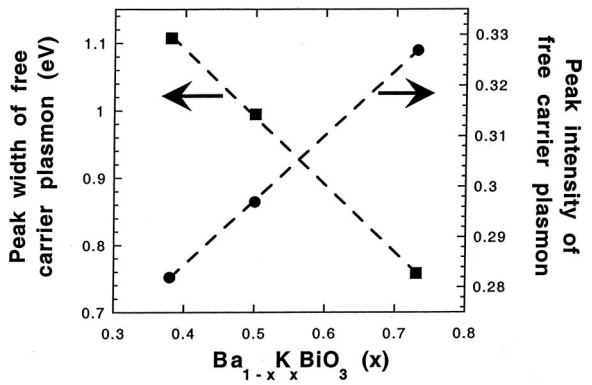

FIG. 3. The free-carrier plasmon is fitted for different K concentration with a Drude model plus a broad excitation as the background. The width of the plasmon peak (square) is plotted against K concentration. The width becomes narrower with increasing K concentration. The maximum intensity (circle) of the free-carrier plasmon peak in the loss function is also shown in the same figure and it increases with increasing K concentration.

not determined for different dopings. (2) We expect some differences between polycrystalline and single-crystalline samples in terms of plasmon intensity.

The energy loss spectra for $x=0.38$, 0.50, and 0.73 are shown in Figs. 4, 5, and 6, respectively. As shown in this figure, an increase in the momentum transfer along [100] and [110] causes a shift towards high energy in the peak position for the ''free-carrier'' plasmon, but with a different dispersion along these two directions. The difference of the dispersion along these two directions gets smaller as the concentration of K increases.

In the 4–6 eV regime, the excitation is mostly isotropic along [100] and along [110] for $x=0.38$ with the highest T_c. With increasing K concentration and lower T_c, the spectra becomes anisotropic along [100] and [110], with strong excitation in the 4–6 eV region along the [100] direction at high momentum transfer. With $x=0.73$ and for T_c less than 4 K, the difference along these two directions is stronger in the

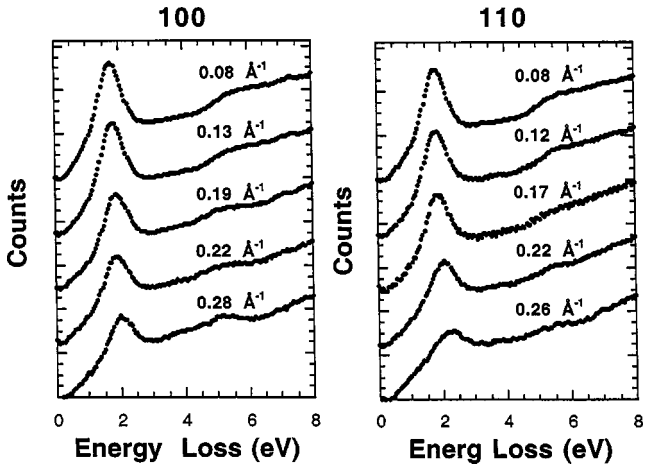

FIG. 5. Energy-loss spectra for BKBO ($x=0.50$) with different momentum transfer **q** along [100] and [110] directions. The magnitude of q is given on the curves in units of Å^{-1}.

4–6 eV region. However, because of our limited data set at higher momentum transfer, we need further experimental work to draw a definitive conclusion of the anisotropic excitation in the 4–6 eV region for the $x=0.73$ K dopant concentration.

The energy peak dispersions of the free-carrier plasmon for different doping levels along different directions are plotted in Fig. 7, where the vertical scale is different for different doping levels. With optimum doping ($x=0.38$), where $T_c=32$ K, the dispersion along [110] is higher than the dispersion along [100]. For this doping level, the effective mass of the free-carrier plasmon along the [100] direction is $1.01m_e$, and the effective mass along [110] is $0.59m_e$, about 40% smaller. With doping at $x=0.50$ and a T_c of 19 K, the anisotropy of the dispersion along [100] and [110] decreases. With a doping level of 0.73 and a T_c of 2 K, the dispersion becomes almost isotropic (the dispersion along [100] is slightly higher).

Figure 8(a) shows the plasmon energy extrapolated to q

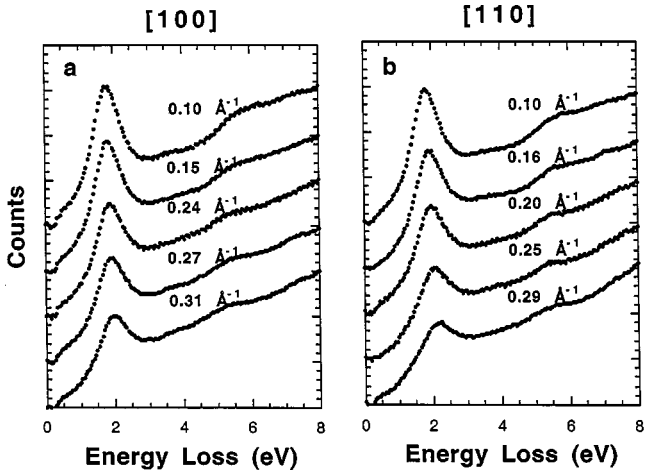

FIG. 4. Energy-loss spectra for BKBO ($x=0.38$) with different momentum-transfer **q** along the [100] and [110] directions. The magnitude of q is given on the curves in units of Å^{-1}.

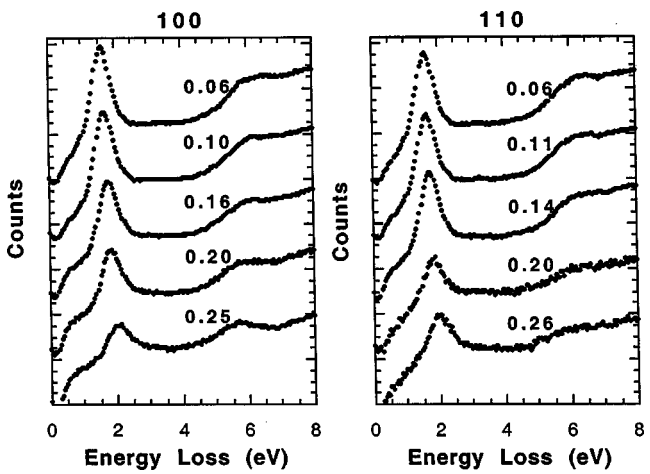

FIG. 6. Energy-loss spectra for BKBO ($x=0.73$) with different momentum-transfer **q** along the [100] and [110] directions. The magnitude of q is given on the curves in units of Å^{-1}.

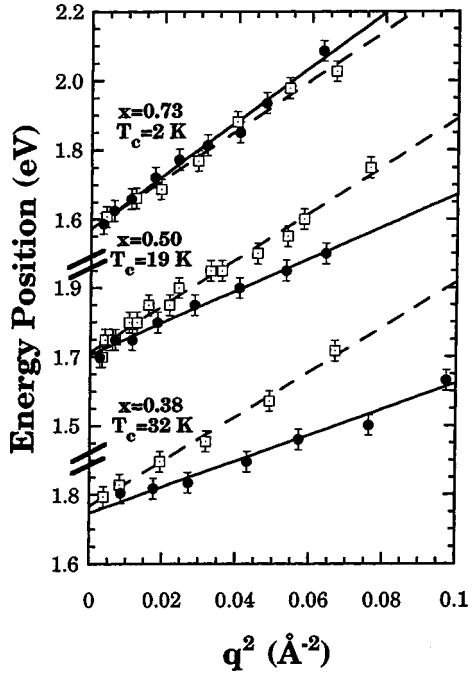

FIG. 7. Free-carrier plasmon energy vs q^2 along [100] and [110] in BKBO with the different doping level ($x=0.38$, 0.50, and 0.73). The solid circle dots and solid line are the data along the [100] direction and square dots and dashed line are the data along the [110] direction. Note: the vertical scale for different doping levels is different.

$=0$ Å^{-1}. For each doping level, there are two data points for the plasmon position derived from two different directions. Within experimental error, these two data points are almost identical for all the doping levels, except there is a small discrepancy for $x=0.38$ doping level, which may be due to the larger experimental error. The plasmon energy position decreases with an increase in K doping. Figure 8(b) shows the different doping levels versus dispersion coefficient α along [100] and [110]. α is defined in the equation $E(q)=E(0)+\alpha\hbar^2q^2/(2m_e)$, where m_e is the bare mass of an electron. The dispersion along [100] increases more rapidly with increasing doping, while the change along the [110] direction is relatively small. Figure 4(c) shows the difference between the dispersion coefficients along [110] and [100]. It is clear that this difference varies between the optimal doped and overdoped cases.

Based on the band structure, the difference in coefficients between these two directions for different doping is calculated and it is compared with experimental data in Fig. 8(c). The detail of the band-structure calculation will be discussed in the following section.

In addition, the T_c versus anisotropy of free-carrier effective mass is extracted from the experimental data and shown in Fig. 9. The linear correlation between T_c and anisotropy of free-carrier effective mass is observed. This difference could be attributed to mass renormalization of the free carrier along different crystal orientations. The significance of this result will be discussed in the following sections.

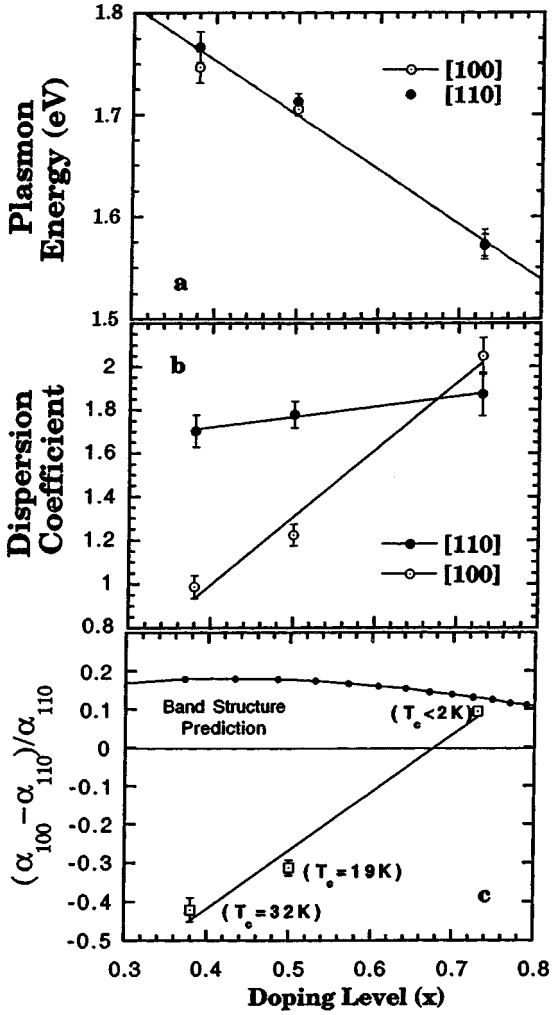

FIG. 8. (a) The plasmon peak position at zero momentum transfer for different doping levels. (b) The free-carrier plasmon dispersion coefficient α along [100] and [110] vs different doping levels. α is defined, as in the following equation: $E(q)=E(0)+\alpha\hbar^2q^2/(2m_e)$. (c) The anisotropic dispersion with doping and its comparison with band-structure calculation. The solid circle dots are the calculation of band structure, and square dots are the experimental data.

IV. DISCUSSION

In this section, we will discuss the comparison between calculation based on a band-structure model and the experimental results. We will show that the band structure alone cannot be used to explain the anisotropic dispersion of the free-carrier plasmon in the optimal doped regime, but it can be used to explain the dispersion of the free-carrier plasmon in the overdoped regime, where T_c goes to almost zero. In order to explain the anisotropic dispersion, we propose a mixing state model of small exciton and free carrier for the optimal doped regime. Because of the linear correlation between T_c and the anisotropy of free-carrier effective mass, based on the proposed model, we conclude that the superconductivity in BKBO may be related to the small exciton, which will be referred to as a WZK exciton.

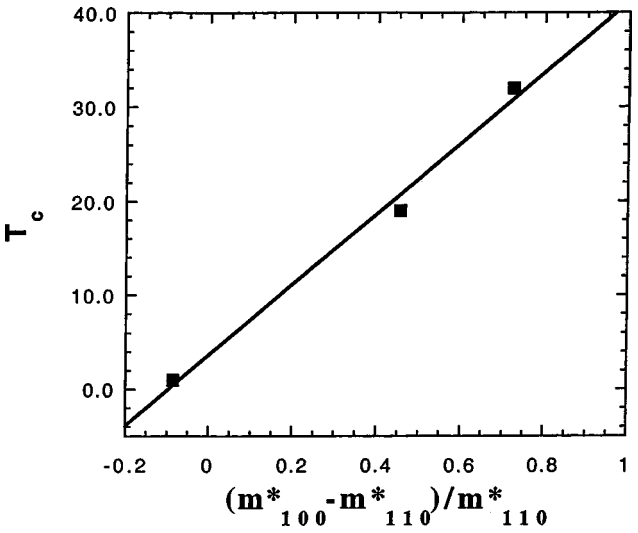

FIG. 9. T_c vs anisotropy of the free-carrier effective mass. In the figure, the T_c decreases as effective mass become more isotropic along the [100] and [110] directions.

A. Band-structure calculation

Following Nucker *et al.*,[11] the plasmon dispersion can be obtained by calculating the dielectric function as follows:

$$\mathrm{Re}\,\varepsilon(\mathbf{q},\omega)=0,$$

$$\varepsilon(\mathbf{q},\omega)=1+\frac{4\pi}{q^2}\chi(\mathbf{q},\omega), \tag{2}$$

where according to the Lindhard-Ehrenreich-Cohen expression,[11] in the long-wavelength limit (or small-q limit), $\chi(\mathbf{q},\omega)$ can be approximately written as

$$\chi(\mathbf{q},\omega)=-\frac{2e^2}{(\hbar\omega)^2}\left[\langle(\mathbf{q}\cdot\mathbf{v})^2\rangle_{\mathrm{FS}}+\frac{\langle(\mathbf{q}\cdot\mathbf{v})^4\rangle_{\mathrm{FS}}}{(\hbar\omega)^2}+\frac{1}{12}\left\langle(\mathbf{q}\cdot\mathbf{v})\left[\mathbf{q}\cdot\frac{\partial}{\partial\mathbf{k}}\right]^2(\mathbf{q}\cdot\mathbf{v})\right\rangle_{\mathrm{FS}}\right]. \tag{3}$$

In this equation, $\mathbf{v}$ is the Fermi velocity,

$$\mathbf{v}=\frac{\partial E_{\mathbf{k}}}{\partial\mathbf{k}}, \tag{4}$$

evaluated for $\mathbf{k}$ on the Fermi surface (FS), and the Fermi surface average is defined by

$$\langle(\cdots)\rangle_{\mathrm{FS}}=\int\frac{d^3k}{(2\pi)^3}\delta(E_{\mathbf{k}}-E_F)(\cdots). \tag{5}$$

The first two terms on the right-hand side of Eq. (3) follow the Boltzmann equation. The last term of Eq. (3) is small and can be neglected. Combining Eqs. (2) and (3), one can show that the first term of Eq. (3) does not contribute to the dispersion because of the cancellation of q^2 and only the second term contributes to the dispersion of the plasmon.

The dispersion is dependent on the integration of the fourth power of the Fermi velocity at the Fermi surface according to Eq. (3). However, because of $\mathbf{q}\cdot\mathbf{v}$ in the integral, the largest contribution to the integral comes from those portions of the Fermi surface where $\mathbf{v}$ is parallel or antiparallel to $\mathbf{q}$. This allows one to use the energy contour map near the Fermi surface to estimate along which direction the dispersion is higher.

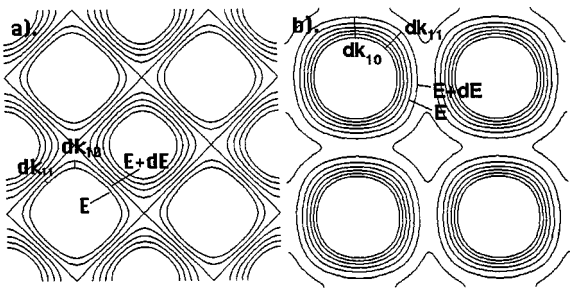

FIG. 10. (a) The energy surface contour map in the k_x-k_y plane with $t_2'/t_1'=0$ of Eq. (8), which is a nearest-neighbor approximation, where only Bi $6s$ and O $2p$ overlap is considered. (b) The energy surface contour map in the k_x-k_y plane with $t_2'/t_1'=0.45$ of Eq. (8), which is a next-nearest-neighbor approximation, where O-O overlap is also included (Ref. 14).

In BKBO, according to the band structure calculation, the Fermi surface at $x=0.29$ doping is fairly isotropic, with a ''square'' Fermi surface turning 45° away from the perfect nesting (half-filled situation).[12] In order to show how the direction of the square Fermi surface affects the dispersion of the free-carrier plasmon, we adopted a commonly used tight-bonding fitting procedure to approximate the Fermi surface near and below half-filling.

According to the band-structure calculation, the strong overlap of Bi $6s$ and O $2p$ orbital is a major contributor to the valence-band structure. The overlap of O $2p$ with neighboring O $2p$ is also another major contributor to the band structure near the Fermi surface. If only the nearest-neighbor interaction (Bi $6s$ and O $2p$ interaction) is considered, the Fermi surface can be approximated by the following equation near the half-filling:

$$E(\mathbf{k})=E_0-2t_1[\cos(k_xa)+\cos(k_ya)+\cos(k_za)]. \tag{6}$$

The contour map of the energy surface in the k_x-k_y plane based on Eq. (6) is shown in Fig. 10(a). This contour map clearly deviates from the band-structure calculation, where the''square'' of the contours is rotated by 45° away from the contours of the band-structure calculation. This shows that simple nearest-neighbor approximation is not a good approximation to mimic the Fermi surface of the band structure.[12–14] By considering next-nearest-neighbor approximation (including the O-O interaction), we can improve Eq. (6),

$$E(\mathbf{k})=E_0-2t_1[\cos(k_xa)+\cos(k_ya)+\cos(k_za)]+4t_2[\cos(k_xa)\cos(k_ya)+\cos(k_ya)\cos(k_za)+\cos(k_za)\cos(k_xa)], \tag{7}$$

to mimic the Fermi surface below half-filling. It should be pointed out that Eq. (7) is used to illustrate the Fermi surface

below half-filling. It cannot be used to approximate the Fermi surface of the band structure above half-filling. For the Fermi surface in k_x-k_y plane, assuming $k_z=0$, we can convert Eq. (7) into the following:

$$E(\mathbf{k})=E_0'-2t_1'[\cos(k_xa)+\cos(k_ya)] + 4t_2'\cos(k_xa)\cos(k_ya), \quad (8)$$

where

$$E_0'=E_0-2t_1, \quad t_1'=t_1-2t_2, \quad t_2'=t_2.$$

The energy surface contour map based on Eq. (8) is calculated near half-filling and shown in Fig. 10(b). It is clear that the Fermi surface based on this approximation is closer to the band-structure calculation, where the square of the Fermi surface is more isotropic and is turned 45° away from the one based on Eq. (6). This difference was pointed out by Yu and co-workers for the cuprate band-structure calculation.[13,14]

Since the dispersion along one particular direction is largely dependent on the Fermi velocity along that direction, according to Eq. (3), by estimating the Fermi velocity from the contour maps along [100] and [110] directions, we can estimate the direction in which the dispersion is larger. Estimating the relative Fermi velocity along different directions from the contour map is fairly simple because the energy difference *dE* between two contour lines is always the same and only *dk* is different, which can be measured on the graph.

For the Fermi surface closer to the band-structure calculation shown in Fig. 10(b), *dk* is more isotropic with slightly smaller *dk* along the [100] direction. Because of smaller *dk* along the [100] direction, this indicates that the Fermi velocity ($v=dE/dk$) along [100] is larger than that along [110]. This translates to a slightly larger dispersion of the free-carrier plasmon along the [100] direction. This is consistent with the numerical calculation based on Eq. (7), where the dispersion is slightly larger along the [100] direction, as shown in Fig. 8(c). Therefore, the experimental results at optimal doping contradict the calculation based on the more realistic band-structure model. The anisotropic dispersion of the plasmon for the superconducting state has a sign opposite from that based on the band-structure calculation, as shown in Fig. 8(c). However, in the overdoped regime, where T_c is almost zero, the dispersion is isotropic and it is closer to the dispersion calculation based on Eq. (7) shown in Fig. 8(c).

These collective results indicate the band-structure calculation can only be used to describe the overdoped material ($T_c \sim 2$ K), but not the optimally doped material ($T_c \sim 32$ K). They imply that additional excitation is needed to explain the anisotropic dispersion of the free-carrier plasmon for optimally doped superconductor. In the following section, we will introduce a small-exciton model in addition to the free carrier to explain the anisotropic dispersion of the free-carrier plasmon for optimally doped case.

It is noted that similar anisotropic dispersion of free carrier plasmon was found in cuprates superconductors by Nucker *et al.*[11] They reported that the effective mass of the free-carrier plasmon along [100] is larger than that along [110]. The larger effective mass of the free-carrier plasmon along [100] is consistent with the observation of a flat band along [100] ($\Gamma-M$) in angle-resolved photoemission experiments.[15] Nucker *et al.*[11] used a simple tight-binding model, namely,

$$E(\mathbf{k})=E_0-2t_1[\cos(k_xa)+\cos(k_ya)], \quad (9)$$

to explain the anisotropic dispersion in the cuprates. However, similar to the above discussion for BKBO, Eq. (9) does not mimic the Fermi surface of the band-structure calculation. As pointed out by Nucker *et al.* in the same paper,[11] in a more realistic band-structure model, the calculations indicate that the dispersion is fairly isotropic, in contrast to the experimental results for cuprate superconductors.[11,13,14] This indicates that in the optimally doped cuprate superconductors, the band structure cannot be used to explain the anisotropic dispersion of the free-carrier plasmon in cuprates, similar to the case of the BKBO superconductor at optimal doping.

B. Anisotropic dispersion in the framework of small excitons

The analysis above indicates that additional interaction is required to explain the anisotropic dispersion of the free-carrier plasmon in the optimal doped region for BKBO. The anisotropy of the free-carrier plasmon found in BKBO is similar to the anisotropic dispersion of *p*-wave excitons found by EELS for the parent insulating compound $BaBiO_3$.[4] This similarity leads us to conjecture that the plasmon dispersion may be related to the small exciton dispersion in the parent insulator via a continuous evolution.

1. Small exciton in the insulating compound $BaBiO_3$

In order to understand the electronic structure of the doped material, we have to understand the electronic structure of the parent compound $BaBiO_3$. Similar to the undoped cuprates, $BaBiO_3$, the parent compound of BKBO, is an insulator despite the prediction from band-structure calculations that it is a metal.[1,2] Owing to the different Bi-O bond lengths, a model involving the charge density wave (CDW) instability has been proposed to explain the insulating nature of $BaBiO_3$.[1–3] However, the anisotropic dispersion of the optical gap, which was reported in the angle-resolved electron-energy-loss spectroscopy experiments, indicates that the CDW model does not apply to this material.[4]

There is an unsettled question of whether the electronic structure of $BaBiO_3$ is similar to that of cuprates. In the cuprate case, it is understood that because of the strong electron repulsion of the Cu *d* orbital, cuprate is a strong coupling system. This Coulomb repulsion of the Cu *d* electron is known as positive *U*. In the $BaBiO_3$ case, however, there is a Coulomb attraction on the Bi site, which favors Bi as +3 instead of +4, with a hole residing at the one of three nearest-neighbor O atoms in the unit cell.[16] This results in a strong coupling system for $BaBiO_3$. The Coulomb attraction in $BaBiO_3$ instead of repulsion is known as a negative *U*.[17] Small-exciton excitation can be described as an electron moving from a Bi site to a neighboring O site as shown in

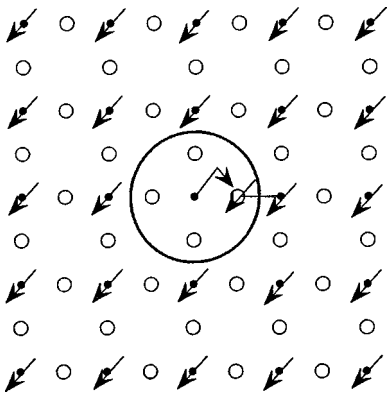

FIG. 11. Small exciton transition between Bi $6s$ and O $2p$. The solid dots represent the Bi atom and the circles represent the O atom. The arrow is to illustrate the electron location. It does not represent the spin of the electron.

Fig. 11. For $BaBiO_3$, the BiO_6 octahedral structure has two additional neighboring oxygen atoms above and below the Bi atom out of the drawing plane in Fig. 11.

By using a wave-function overlapping argument similar to that in Refs. 5 and 18, we can carry out a matrix calculation for $BaBiO_3$, considering a small-exciton transition from O $2p_\sigma$ to Bi $6s$ as shown in Fig. 11. Denoting the hole hopping matrix element between Bi $6s$ and O $2p_\sigma$ with overlapping energy as $t_{sp\sigma}$ and the hole hopping matrix between neighboring O $2p_\sigma$ as t_{pp}, we can construct a 6×6 matrix (see the Appendix). This matrix can be easily solved, giving three different energy levels, with one s state, three p states, and two d states: $d(x^2-y^2)$ and $d(3z^2-r^2)$. The s state has the highest energy, the p states are in the middle, and the d states are the lowest.

The small exciton was observed and proposed in the angle-resolved EELS spectra of $Sr_2CuO_2Cl_2$ and $BaBiO_3$ by Wang, Zhang, Klein, and their colleagues.[4,5,18,19] We can refer this kind of exciton as a WZK exciton. For convenience, we define three branches of excitons as W excitons with the lowest energy, Z excitons in the middle, and K excitons with the highest energy. For undoped BKBO and cuprates, the W exciton is the d exciton, the Z exciton is the p exciton, and the K exciton is the s exciton. The weak excitation centered at 0.4 eV observed by optical absorption measurement in the cuprate insulators can be assigned to the optically forbidden W exciton.[5,20,21]

Since the ground state in $BaBiO_3$ has s symmetry, only the s to p transition is dipole allowed. Both the s-wave exciton and the d-wave exciton are dipole forbidden. The forbidden transition of the K exciton was observed along [100] with a high momentum transfer at 4.2 eV. This is because in that state there is a wave function mixing between s and p waves resulting in the dipole oscillator strength transferring from the 2.1 eV state to the 4.2 eV state at high momentum transfer, which was confirmed by the EELS experiment.[22]

Another optically forbidden state, the W exciton, in the insulator compound at low energy is in the d state and cannot be observed by normal optical reflectance measurement. However, it can be measured through optical absorption as a weak dipole-allowed transition with slightly broken symmetry due to the imperfections of crystal structure and acoustic vibration, which results in a small wave function mixing of the dipole-allowed state into the W exciton. Infrared absorption measurements from $BaBiO_3$ reveal a broad weak state centered at 0.5 eV,[22,23] which can be assigned as the optically forbidden state, the d-wave exciton.

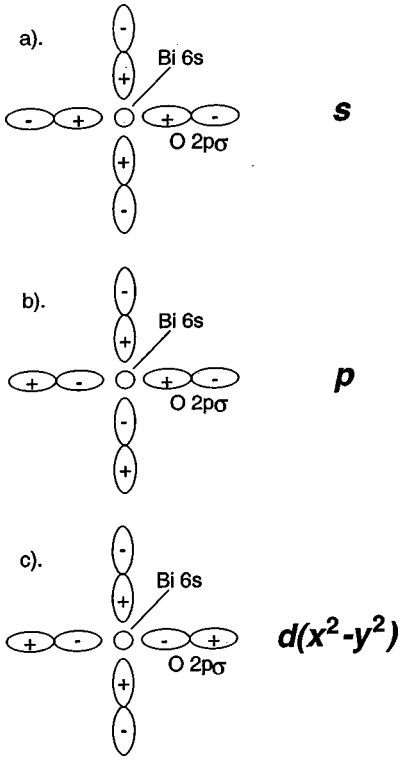

FIG. 12. (a) Wave function of the s-symmetry exciton; (b) wave function of p-symmetry exciton; (c) wave function of $d(x^2-y^2)$-symmetry exciton.

The examples of the symmetries of the s-wave, p-wave, and d-wave exciton are shown in Fig. 12. Some light doping without free carriers in BKBO is not expected to change the symmetry of the exciton. If there is a mixing of free carriers and the small exciton, there will be wave function mixing between s, p, and d states even at $q=0$ due to the charge fluctuations caused by the free carriers. This results in significant wave function redistribution among the W exciton, Z exciton, and K exciton.

2. Excitation in middle-infrared region with free carriers

As reported by Karlow *et al.*,[24] for a doping level of $x=0.38$, there is a Drude-type excitation at zero energy, with a broad feature in the midinfrared region. The middle-infrared feature can be attributed as a dipole-allowed transition of the W exciton due to the change of the symmetry in the presence of free carrier. With increasing doping level to $x=0.51$, the intensity of midinfrared excitation decreases, and at the same time, T_c decreases also. However, because of strong tail of Drude-type excitations in the midinfrared region, it was not able to detect weakened midinfrared excitation with overdoping of $x=0.51$. Therefore, the optical method is not a sensitive technique to observe midinfrared

excitation in the overdoped region due to strong background of Drude oscillation from the free carrier in the middle-infrared region.

In cuprates, similar oscillator strength transferring from the excitation in the 1.6–2.0 eV range in the cuprate insulator compound to the middle-infrared region through the free-carrier dopant in the superconductor compound has been widely reported and extensively discussed by many authors.[25–27]

3. Renormalization of the free-carrier effective mass

In the picture of the small exciton, because of interaction between the free carrier and small exciton, the effective mass of the free carrier is renormalized. Since the mass of the small exciton is heavier along the [100] direction, and light along the [110] direction, the interaction between the small exciton and free carrier results in a heavier effective mass of the free carrier along the [100] direction and a light mass along the [110] direction. The effective mass anisotropy of the free carrier can be used as a gauge to indicate whether there is an interaction between the small exciton and free carrier. This method is more sensitive than the optical method discussed above.

Increasing K doping results in more free carriers and reduces the strength of the small exciton due to the screening effect. This in turn gives rise to a weaker interaction between electrons through the interaction of the small exciton and leads to less mass renormalization of free carrier, especially along the [100] direction. When the material is highly overdoped, the mass renormalization of the free carrier totally disappears, which implies that the interaction between the small exciton and free carrier is almost zero. It is extremely interesting that T_c is proportional to the effective-mass renormalization of the free carrier as shown in Fig. 9.

A similar anisotropy of free-carrier mass renormalization is also reported in cuprates for slightly overdoped material with a T_c of 87 K.[11] It would be interesting to see how the anisotropic dispersion behaves under the extremely overdoped condition where T_c goes to zero for cuprate superconductors.

C. Other dielectric function changes with K concentration

In addition to the change of the free-carrier plasmon dispersion with the change of K concentration, the change of free-carrier plasmon width and intensity with the change of K concentration also provides consistent evidence that there is less of middle-infrared excitation with increasing K concentration. There are two ways to explain the width and intensity change in terms of middle-infrared excitation. First, the measured free-carrier plasmon consists of free-carrier plasmon excitation and middle-infrared excitation. The width of the peak represents the combined result of free-carrier plasmon and middle-infrared excitation. With increasing K concentration, the strength of middle-infrared excitation is reduced, which leads to a smaller width and higher intensity of the measured free-carrier plasmon. The second reason for this relationship can be attributed to the interaction between the free-carrier plasmon and middle infrared excitation, which leads to the broadening of the free-carrier plasmon peak. However, regardless of interpretation of the data, the conclusion of lower middle-infrared excitation at higher K concentration is still valid. Furthermore, we also noticed the change in the dielectric function with K concentration shown in Fig. 2 and the change of anisotropic excitation in the 4–6 eV energy region with K concentration shown in Figs. 4–6.

V. CONCLUSION

In summary, we have performed **q**-resolved EELS measurements on the BKBO superconductor for various doping levels. In the optimum doped material, the effective mass of the ''free-carrier'' plasmon is heavy along [100] and light along [110] (the dispersion is smaller along [100] and larger along [110]), while in the over doped material the effective mass is almost isotropic along [100] and [110]. We also reported a linear correlation between T_c and mass renormalization of free-carrier plasmon. In this paper, we proposed a mixing state of a free carrier and small exciton in the optimally doped region for the BKBO superconductor. The disappearance of the anisotropy dispersion of the free-carrier plasmon in the overdoped material, where T_c goes to almost zero, provides evidence that the superconductivity in BKBO is very likely to be related to the electronic structure, and possibly to the small exciton (WZK exciton).

ACKNOWLEDGMENT

We would like to thank M. V. Klein, V. P. Dravid, D. A. Payne, and F. C. Zhang for stimulating discussions. We would also like to acknowledge the band contour map plotted by H. Wildman of IBM Micro-electronic Division at East Fishkill, NY. The research is supported by the NSF-DMR through the Science and Technology Center for Superconductivity under Grant No. DMR-91-20000.

APPENDIX: CALCULATION OF THE SMALL EXCITON STATE FOR $BaBiO_3$

The small exciton transition can be described as electron moving from a Bi site to a neighboring O site as shown in Fig. 11. The existence of this small exciton is due to the fact that there is a strong Coulumb attraction of the Bi electron, which makes Bi^{3+} more favorable than Bi^{4+}, with a hole residing at three neighboring O atoms in one unit cell. This Coulumb attraction is known as a negative U.[17]

Because of the $BaBiO_3$ cubic structure with the BiO_6 octahedral structure, according to the Hucker expression,[28,29] the exciton state with $q=0$ can be described by the following matrix:

$$\begin{array}{c|cccccc} & P_x & P_y & P_z & P_{-x} & P_{-y} & P_{-z} \\ P_x & t_2 & t_1 & t_1 & t_2 & t_1 & t_1 \\ P_y & t_1 & t_2 & t_1 & t_1 & t_2 & t_1 \\ P_z & t_1 & t_1 & t_2 & t_1 & t_1 & t_2 \\ P_{-x} & t_2 & t_1 & t_1 & t_2 & t_1 & t_1 \\ P_{-y} & t_1 & t_2 & t_1 & t_1 & t_2 & t_1 \\ P_{-z} & t_1 & t_1 & t_2 & t_1 & t_1 & t_2 \end{array}, \tag{A1}$$

where

$$t_1 = t_{pp} - t_{sp}^2/\varepsilon_p, \quad t_2 = -t_{sp}^2/\varepsilon_p. \tag{A2}$$

By solving this matrix, we can obtain six states: one S state as E_+, two D states as E_-, and three P states as E, where

$$E_+ = 4t_{pp} - 6t_{sp}^2/\varepsilon_p \quad (S),$$

$$E = 0 \quad (P_1, P_2, P_3),$$

$$E_- = -2t_{pp} \quad (D_1, D_2). \tag{A3}$$

Because the ground state is an S state for $BaBiO_3$, only three P states are optically allowed for $q=0$, and E_+ and E_- states are both optically forbidden states for $q=0$. The forbidden states are observed by EELS and infrared absorption measurements. According to the measurement, we can assign the 4.2 eV optically forbidden state as the S state, 2.1 eV optically allowed state as three P states, and 0.5 eV forbidden state (observed by infrared absorption as a weak state) as two D states.[22,23] This results in $E_+ = 2.1$ eV and $E_- = 1.6$ eV, which in turn results in

$$t_{pp} = 0.8 \text{ eV},$$

$$t_{sp}^2/\varepsilon_p = 0.18 \text{ eV}. \tag{A4}$$

After the calculation, in D, P, S space, the matrix (A1) can be rewritten as

$$\begin{array}{c|cccccc} & D_1 & D_2 & P_1 & P_2 & P_3 & S \\ D_1 & E_- & 0 & 0 & 0 & 0 & 0 \\ D_2 & 0 & E_- & 0 & 0 & 0 & 0 \\ P_1 & 0 & 0 & E & 0 & 0 & 0 \\ P_2 & 0 & 0 & 0 & E & 0 & 0 \\ P_3 & 0 & 0 & 0 & 0 & E & 0 \\ S & 0 & 0 & 0 & 0 & 0 & E_+ \end{array} . \tag{A5}$$

This indicates that at $q=0$ with perfect symmetry, there is no wave function mixing between D,P,S wave excitons (WZK exciton). Mathematically, if the nondiagonal matrix is not zero, such as M_{PD} is not zero, there will be wave-function mixing between P and D states, which would result in a dipole-allowed transition at D-exciton energy. For convenience, we can define the low-energy exciton as the W exciton, the one in the middle as Z exciton, and the highest-energy exciton as the K exciton.

If the motion of the small exciton is considered, the matrix symmetry depends on the direction of the motion for the small exciton. For the [111] direction, the symmetry remains the same as $q=0$, which implies that there will be no mixing state between two D states, three P states, and S state. Along the [110] direction, the symmetry of the matrix is slightly broken, and there will be some wave-function mixing between D, P, and S states. Along the [100] direction, the symmetry is strongly broken, and this results in a strong wave-function mixing between D, P, and S states. Because of wave-function mixing, the forbidden transition would have dipole-allowed components in these states, which makes the forbidden transition visible at that energy level with the motion of the exciton ($q \neq 0$). This is one reason why we observed a strong forbidden transition at 4.2 eV along the [100] direction, a weak forbidden transition along the [110] direction, and no forbidden transition along the [111] direction.[4] The detailed calculation of wave-function mixing at finite q is beyond the scope of this work. The wave-function mixing calculation at finite q was performed on the insulator cuprate case, where similar properties of forbidden transitions were observed.[5,18] Cuprate has a two-dimensional structure instead of three-dimensional. The motion of the small exciton along [110] direction keeps the symmetry the same as $q=0$, and no forbidden transition was observed along that direction. Along the [100] direction, the motion of the small exciton causes the symmetry of the matrix to be broken, which results in strong wave-function mixing between P and S states, which in turn results in a strong forbidden transition along the [100] direction at higher energy (K exciton). In the presence of the free carrier, the wave function between the W exciton, Z exciton, and K exciton would be in the mixing state of S, P, D waves.

*Present address: IBM, Zip 40E, 2070 Route 52, Hopewell Junction NY 12533-6531. Electronic address: WANGYY@US.IBM.COM

[1] D. E. Cox and A. W. Sleight, Solid State Commun. **19**, 969 (1976).
[2] L. F. Schneemeyer, J. K. Thomas, T. Siegrist, B. Batlog, L. W. Rupp, R. L. Opila, R. J. Cava, and D. W. Murphy, Nature (London) **335**, 421 (1988).
[3] M. J. Rice and Y. R. Wang, Physica C **157**, 192 (1989).
[4] Y. Y. Wang, V. P. Dravid, N. Bulut, P. D. Han, M. V. Klein, S. E. Schnatterly, and F. C. Zhang, Phys. Rev. Lett. **75**, 2546 (1995).
[5] Y. Y. Wang, F. C. Zhang, V. P. Dravid, K. K. Ng, M. V. Klein, S. E. Schnatterly, and L. L. Miller, Phys. Rev. Lett. **77**, 1809 (1996).
[6] D. G. Hinks, MRS Bull. **15** (6), 55 (1990).
[7] P. D. Han *et al.*, J. Cryst. Growth **128**, 798 (1993).
[8] P. D. Han (unpublished).
[9] Y. Y. Wang, S. C. Cheng, V. P. Dravid, and F. C. Zhang, Ultramicroscopy **59**, 109 (1995).
[10] Y. Y. Wang, H. Zhang, V. P. Dravid, D. Shi, D. G. Hinks, Y. Zheng, and J. D. Jorgensen, Phys. Rev. B **47**, 14 503 (1993).
[11] N. Nucker, U. Eckern, J. Fink, and P. Muller, Phys. Rev. B **44**, 7155 (1991).
[12] N. Hamada, S. Massidda, and A. J. Freeman, Phys. Rev. B **40**, 4442 (1989).
[13] J. Yu, S. Massidda, and A. J. Freeman, Physica C **152**, 273 (1988).
[14] J. Yu and A. J. Freeman, J. Electron Spectrosc. Relat. Phenom. **66**, 281 (1993).
[15] S. D. Dessau, Z. X. Shen, D. M. King, D. S. Marshell, L. W. Lambardo, P. H. Dickinson, A. G. Loeser, J. D. Carlo, C. H. Park, A. Kapitulnik, and W. E. Spicer, Phys. Rev. Lett. **71**, 2781 (1993).

[16] Z. X. Shen, P. A. P. Lindberg, P. O. Wells, D. S. Dessau, A. Borg, L. Lindau, W. E. Spicer, W. P. Ellis, G. H. Kwei, K. C. Ott, J.-S. Kang, and J. W. Allen, Phys. Rev. B **40**, 6912 (1989).
[17] C. M. Varma, Phys. Rev. Lett. **61**, 2713 (1988).
[18] F. C. Zhang and K. K. Ng, Phys. Rev. B **58**, 13 520 (1998).
[19] Y. Y. Wang, F. C. Zhang, and M. V. Klein (private communication); and (unpublished).
[20] J. D. Perkins, J. M. Graybeal, M. A. Kastner, R. J. Birgeneau, J. P. Falck, and M. Greven, Phys. Rev. Lett. **71**, 1621 (1993).
[21] R. Lovenich, A. B. Schumacher, J. S. Dodge, D. S. Chemla, and L. L. Miller, Phys. Rev. B **63**, 235104 (2001).
[22] Y. Y. Wang (unpublished).
[23] M. E. Kozlov, X. Ji, H. Minami, and H. Uwe, Phys. Rev. B **56**, 12 211 (1997).
[24] M. A. Karlow, S. L. Cooper, A. L. Kotz, M. V. Klein, P. D. Han, and D. A. Payne, Phys. Rev. B **48**, 6499 (1993).
[25] S. Uchida, T. Ido, H. Takagi, T. Arima, Y. Tokura, and S. Tajima, Phys. Rev. B **43**, 7942 (1991).
[26] S. L. Cooper, D. Reznik, A. Kotz, M. A. Karlow, R. Liu, M. V. Klein, W. C. Lee, J. Giapintzakis, and D. M. Ginsberg, Phys. Rev. B **47**, 8233 (1993).
[27] N. M. Plakida, *High-Temperature Superconductivity: Experiment and Theory* (Springer-Verlag, Berlin, 1995).
[28] D. C. Harris and M. D. Bertolucci, *Symmetry and Spectroscopy: An Introduction to Vibration and Electronic Spectroscopy* (Oxford University Press, New York, 1978).
[29] W. A. Harrison, *Electronic Structure and the Properties of the Chemical Bond* (Freeman, San Francisco, 1980).